0090-9556/10/3805-871–878$20.00
DRUG METABOLISM AND DISPOSITION
Vol. 38, No. 5
30817/3575039
DMD 38:871–878, 2010
Printed in U.S.A.

Metabolism-Mediated Drug Interactions Associated with Ritonavir-Boosted Tipranavir in Mice

Feng Li, Laiyou Wang, Grace L. Guo, and Xiaochao Ma

Department of Pharmacology, Toxicology and Therapeutics, University of Kansas Medical Center, Kansas City, Kansas

Received October 14, 2009; accepted January 26, 2010

ABSTRACT:

Tipranavir (TPV) is the first nonpeptidic protease inhibitor used for the treatment of drug-resistant HIV infection. Clinically, TPV is coadministered with ritonavir (RTV) to boost blood concentrations and increase therapeutic efficacy. The mechanism of metabolism-mediated drug interactions associated with RTV-boosted TPV is not fully understood. In the current study, TPV metabolism was investigated in mice using a metabolomic approach. TPV and its metabolites were found in the feces of mice but not in the urine. Principal component analysis of the feces metabolome uncovered eight TPV metabolites, including three monohydroxylated, three desaturated, one dealkylated, and one dihydroxylated. In vitro study using human liver microsomes recapitulated five TPV metabolites, all of which were suppressed by RTV. CYP3A4 was identified as the primary enzyme contributing to the formation of four TPV metabolites (metabolites II, IV, V, and VI), including an unusual dealkylated product arising from carbon-carbon bond cleavage. Multiple cytochromes P450 (2C19, 2D6, and 3A4) contributed to the formation of a monohydroxylated metabolite (metabolite III). In vivo, RTV cotreatment significantly inhibited eight TPV metabolic pathways. In summary, metabolomic analysis revealed two known and six novel TPV metabolites in mice, all of which were suppressed by RTV. The current study provides solid evidence that the RTV-mediated boosting of TPV is due to the modulation of P450-dependent metabolism.

Tipranavir (TPV) is a nonpeptidic HIV protease inhibitor (PI) displaying high enzymatic inhibition and potent antiviral activity. TPV was approved by the Food and Drug Administration in 2005 and extended for pediatric use in 2008. TPV exhibits a different therapeutic profile from that of other currently available PIs, rendering it a potential option for treatment-experienced patients with resistance to multiple PIs (Pham, 2005; Courter et al., 2008). Systematic bioavailability of TPV is low. Clinically, TPV is administered orally twice daily and must be given in combination with low-dose ritonavir (RTV) to boost TPV bioavailability (Cahn et al., 2006). RTV was originally developed as an HIV protease inhibitor. It is now rarely used for its antiviral activity, but it is used as a cytochrome P450 (P450) inhibitor to boost other PIs (Kempf et al., 1997; Hsu et al., 1998). In a phase I clinical trial with healthy adult volunteers, it was noted that coadministration of TPV and RTV (TPV/r) resulted in a significant increase in steady-state TPV trough concentrations compared with TPV at a steady state alone. The means of the TPV trough concentrations were above a preliminary target threshold with most of the RTV-boosted doses. Without the RTV coadministration, none of the TPV-alone doses exceeded the threshold (MacGregor et al., 2004).

This work was supported by the National Institutes of Health National Center for Research Resources [Grant COBRE 5P20-RR021940].

Article, publication date, and citation information can be found at http://dmd.aspetjournals.org.

doi:10.1124/dmd.109.030817.

The mechanism of drug-drug interactions associated with RTV-boosted TPV is not fully understood. An in vitro study with human liver microsomes (HLM) suggested that CYP3A4 is the predominant enzyme involved in TPV metabolism. RTV strongly inhibits CYP3A4, and it was thus proposed that the boosted level of TPV by RTV was mediated by CYP3A4 inhibition (MacGregor et al., 2004; McCallister et al., 2004). Illustration of TPV metabolic pathways would provide valuable information for this proposal. In a recent study using Sprague-Dawley rats, the rats were administered a single dose of [^{14}C]TPV with coadministration of RTV. The most abundant metabolite in feces was an oxidation metabolite. In urine, no single metabolite was found to be significantly present (Macha et al., 2007). In a human study, subjects received 500 mg of TPV with 200 mg of RTV twice daily for 6 days. On day 7, these subjects received a single oral dose of 551 mg of TPV containing 90 μCi of [^{14}C]TPV with 200 mg of RTV, followed by twice-daily 500-mg doses of unlabeled TPV with 200 mg of RTV for up to 20 days. Metabolites were identified using a flow scintillation analyzer in conjunction with liquid chromatography-tandem mass spectrometry. The most abundant metabolite in feces was identified as an oxidation metabolite, whereas a TPV glucuronide metabolite was identified in urine (Chen et al., 2007b). In these two studies, two monohydroxylation metabolites, a dehydrogenation metabolite, and a glucuronide conjugate metabolite of TPV were observed (Chen et al., 2007b; Macha et al., 2007). However, neither the contributions of P450s in TPV metabolism nor the effects of RTV on TPV metabolism are clear.

ABBREVIATIONS: TPV, tipranavir; PI, protease inhibitor; RTV, ritonavir; P450, cytochrome P450; TPV/r, tipranavir and ritonavir; HLM, human liver microsomes; UPLC, ultraperformance liquid chromatography; TOFMS, time-of-flight mass spectrometry; MLM, mouse liver microsomes; PBS, phosphate-buffered saline; rcf, relative centrifugal force; PCA, principal components analysis; OPLS-DA, orthogonal projection to latent structures-discriminant analysis; MS/MS, tandem mass spectrometry.

Metabolomics is a rapid and systematical study of small molecule metabolites found in an organism (Thomas, 2001; Weckwerth, 2003). By integrating the resolving power of ultraperformance liquid chromatography (UPLC) with the accurate mass determination of time-of-flight mass spectrometry (TOFMS) and multivariate data analysis, it is possible to determine the small changes in the metabolome that take place in different groups of organisms (Chen et al., 2007a). The implication of this new technology in drug metabolism has been well established, for example, the metabolomic analysis of aminoflavone, areca alkaloids, and melatonin (Chen et al., 2006; Giri et al., 2006; Ma et al., 2008). In these studies, a number of novel metabolites were discovered. In the current study, the metabolomic approach was used to study TPV metabolism. The role of P450s in metabolic pathways of TPV was determined by using cDNA-expressed human P450s. In addition, the inhibitory effect of RTV on TPV metabolism and distribution was investigated.

Materials and Methods

Chemicals and Reagents. Tipranavir (*N*-{3-[(1*R*)-1-[(2*R*)-6-hydroxy-4-oxo-2-(2-phenylethyl)-2-propyl-3,4-dihydro-2*H*-pyran-5-yl]propyl]phenyl}-5-(trifluoromethyl)pyridine-2-sulfonamide) and ritonavir (1,3-thiazol-5-ylmethyl *N*-[(2*S*,3*S*,5*S*)-3-hydroxy-5-[(2*S*)-3-methyl-2-{[methyl({[2-(propan-2-yl)-1,3-thiazol-4-yl]methyl})carbamoyl]amino}butanamido]-1,6-diphenylhexan-2-yl]carbamate) were supplied by the National Institutes of Health AIDS Research and Reference Reagent Program. The recombinant human P450s and HLM were purchased from XenoTech, LLC (Lenexa, KS). NADPH was obtained from Sigma-Aldrich (St. Louis, MO). All the solvents for liquid chromatography and mass spectrometry were of the highest grade commercially available.

Animals and Treatments. All mice (2–4 months old) were maintained under a standard 12-h dark and 12-h light cycle with water and chow provided ad libitum. Handling was in accordance with study protocols approved by the University of Kansas Medical Center Institutional Animal Care and Use Committee. For metabolomic analysis, TPV (40 mg/kg) was administered via ball-tipped gavage needles, and the mice were housed in separate metabolic cages for 18 h. Urine and feces samples were collected and stored at −20°C for further analysis. For tissue distribution and inhibition studies, three groups of mice were used and were orally treated with TPV (100 mg/kg), RTV (40 mg/kg), and TPV/r (100 mg/kg TPV and 40 mg/kg RTV), respectively. Tissues including the liver, brain, lung, kidney, spleen, and eyes were collected 30 min after treatment and stored at −20°C for further analysis.

Incubation of TPV in HLM, MLM, and Recombinant P450s. The incubation was conducted in 1× phosphate-buffered saline (PBS) (pH 7.4), containing 50 μM TPV, 0.1 mg of HLM or 0.1 mg of MLM or 2 pmol of each cDNA-expressed P450 enzyme (control, CYP1A2, 2A6, 2B6, 2C8, 2C9, 2C19, 2D6, 2E1, and CYP3A4) in a final volume of 200 μl. After 5 min of preincubation at 37°C, the reaction was initiated by the addition of 10 μl of 20 mM NADPH (final concentration 1.0 mM) and continued for 30 min with gentle shaking. The same experiment was performed without NADPH. All reactions were terminated by adding 200 μl of acetonitrile.

Inhibition by RTV on TPV Metabolism In Vitro. RTV (0–100 μM) was used for the inhibitory test. The coincubation of RTV (0.01, 0.1, 1, 10, 20, 50, and 100 μM, separately) was performed in 1× PBS (pH 7.4) containing 50 μM TPV and 0.1 mg of HLM in a final volume of 200 μl. After 5 min of preincubation at 37°C, the reaction was initiated by the addition of 10 μl of 20 mM NADPH (final concentration 1.0 mM) and continued for 30 min with gentle shaking. The preincubation of RTV (1.0, 20, and 50 μM) was carried out in PBS (1×, pH 7.4) containing 0.1 mg of HLM or MLM or 2 pmol of P450 (2C19, 2D6, or 3A4) and 1.0 mM NADPH in a final volume of 198 μl. After 30 min of incubation, 2.0 μl of TPV (final concentration 50 μM) was added, and the resulting mixture was further incubated for 30 min. All reactions were terminated by adding 200 μl of acetonitrile.

Sample Preparation. Urinary samples were prepared by mixing 40 μl of urine with 160 μl of 50% acetonitrile and were centrifuged at 20,000 relative centrifugal force (rcf) for 10 min. Feces were homogenized by adding 1× PBS (1 mg of feces in 10 μl of PBS). Subsequently, 200 μl of acetonitrile was added to 200 μl of the resulting mixture, followed by vortexing and centrifugation at 20,000 rcf for 10 min. The supernatant was transferred to a new Eppendorf vial for a second centrifugation (20,000 rcf for 10 min). Serum samples were prepared by mixing 75 μl of serum with 75 μl of acetonitrile, followed by vortexing and centrifugation at 15,000 rcf for 10 min. Various tissues (brain, liver, kidney, lung, spleen, and eyes) were weighed and homogenized in water (100 mg of tissues in 400 μl of water). Then 100 μl of each mixture was added to 100 μl of acetonitrile, followed by vortexing and

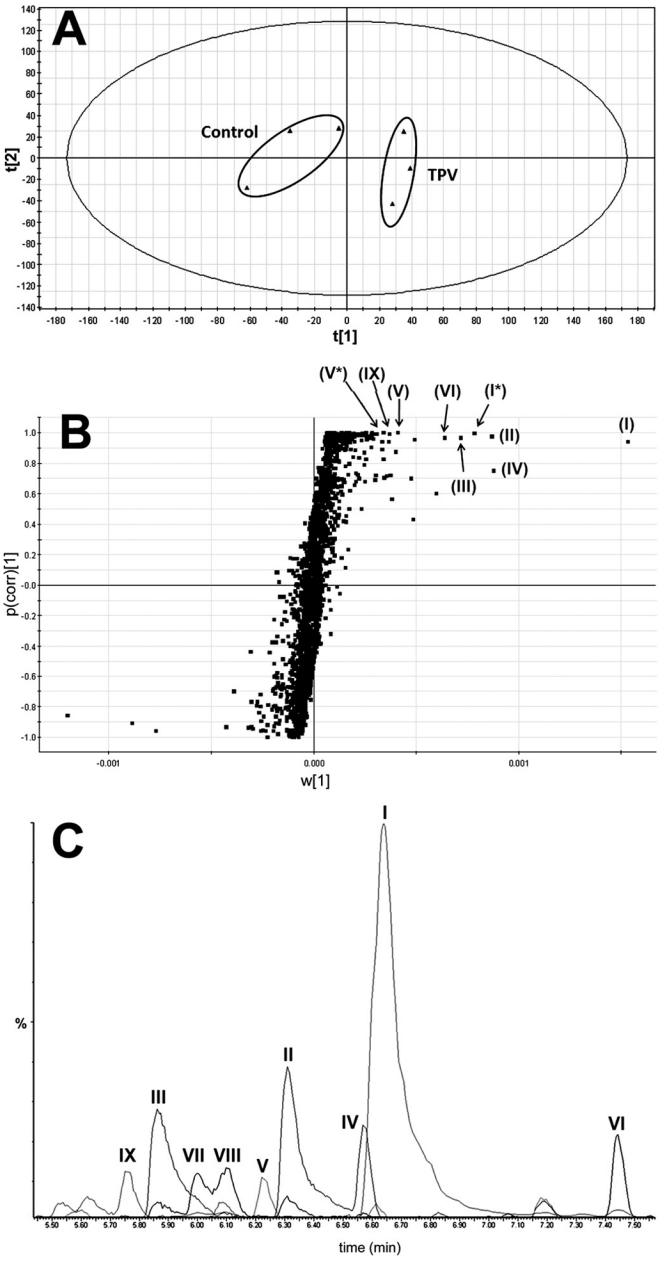

FIG. 1. Metabolomic analysis of control and TPV-treated mouse feces. Wild-type mice ($n = 3$) were treated with 40 mg/kg TPV p.o., and 18-h urine and feces samples were collected for analysis. A, separation of control and TPV-treated mouse feces in PCA scores plot. The t[1] and t[2] values represent the scores of each sample in principal component 1 and 2, respectively. B, loading S-plot generated by OPLS-DA analysis. The *x*-axis is a measure of the relative abundance of ions, and the *y*-axis is a measure of the correlation of each ion to the model. These loading plots represent the relationship between variables (ions) in relation to the first and second components present in A. Top ranking ions are marked. *, sodium adduct of original ion. The number of ions (metabolite identification) was accordant with that in Figs. 2 and 6. C, the chromatograms of TPV and its metabolites: I (TPV); II, III, and IV (monohydroxylated metabolite); V (dealkylated metabolite); VI, VII, and VIII (dehydrogenated metabolites); and IX (dihydroxylated metabolite).

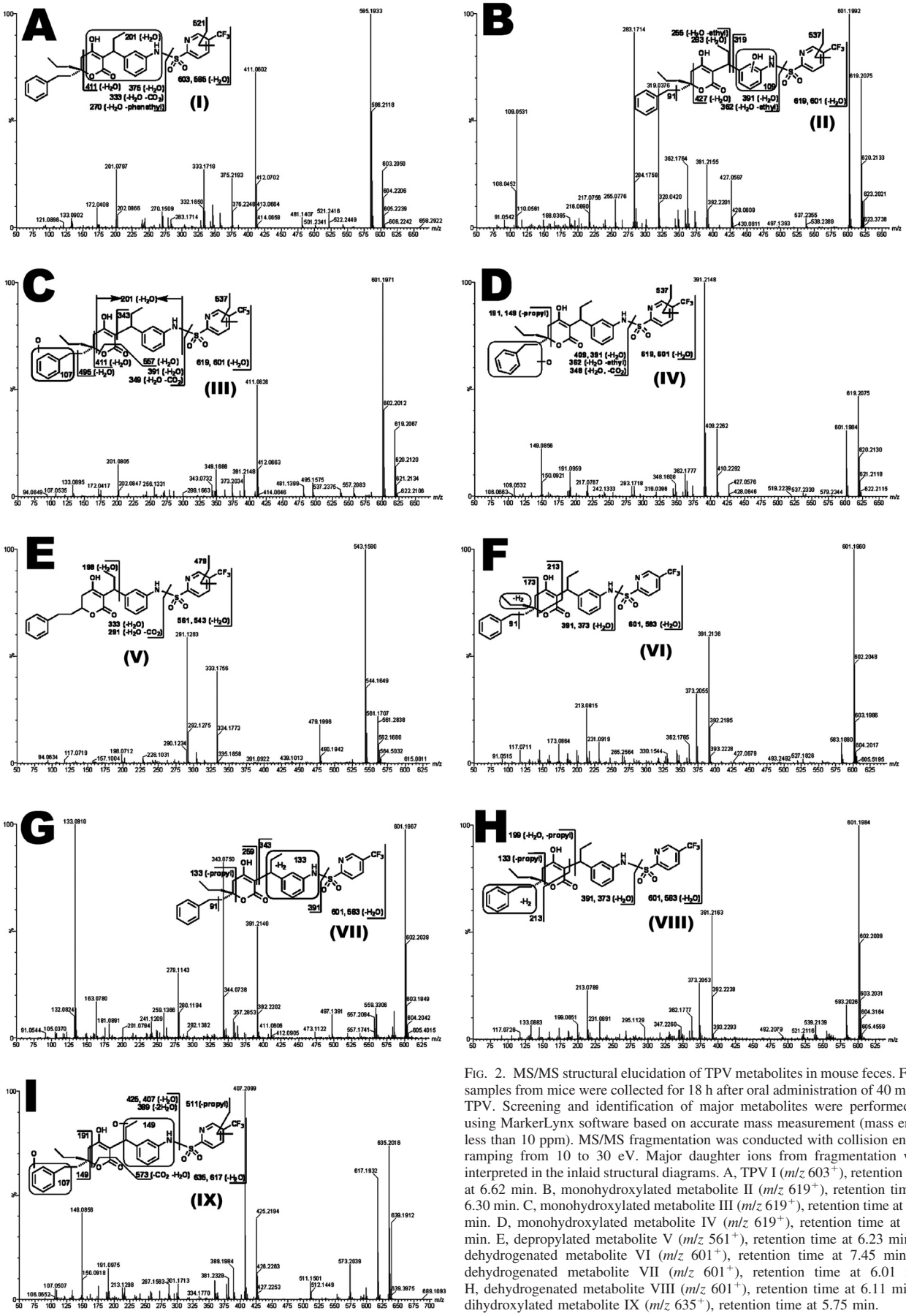

FIG. 2. MS/MS structural elucidation of TPV metabolites in mouse feces. Feces samples from mice were collected for 18 h after oral administration of 40 mg/kg TPV. Screening and identification of major metabolites were performed by using MarkerLynx software based on accurate mass measurement (mass errors less than 10 ppm). MS/MS fragmentation was conducted with collision energy ramping from 10 to 30 eV. Major daughter ions from fragmentation were interpreted in the inlaid structural diagrams. A, TPV I (m/z 603^+), retention time at 6.62 min. B, monohydroxylated metabolite II (m/z 619^+), retention time at 6.30 min. C, monohydroxylated metabolite III (m/z 619^+), retention time at 5.87 min. D, monohydroxylated metabolite IV (m/z 619^+), retention time at 6.58 min. E, depropylated metabolite V (m/z 561^+), retention time at 6.23 min. F, dehydrogenated metabolite VI (m/z 601^+), retention time at 7.45 min. G, dehydrogenated metabolite VII (m/z 601^+), retention time at 6.01 min. H, dehydrogenated metabolite VIII (m/z 601^+), retention time at 6.11 min. I, dihydroxylated metabolite IX (m/z 635^+), retention time at 5.75 min.

centrifugation at 20,000 rcf for 10 min. The supernatant was transferred to a new Eppendorf vial for a second centrifugation (20,000 rcf for 10 min). The extraction recoveries of TPV and RTV have been performed in different tissues, and the extraction rates across the tissues are comparable. The in vitro incubation was terminated by adding 200 μl of acetonitrile and vortexed for 1 min and centrifuged at 20,000 rcf for 10 min. Each supernatant was transferred to an autosampler vial, and 5 μl was injected to a system (Waters, Milford, MA) combining UPLC and TOFMS for metabolite analysis.

UPLC-TOFMS Analysis. A 100 mm $\times$ 2.1 mm (Acquity 1.7 μm) UPLC BEH C-18 column (Waters) was used for metabolite separation. The flow rate of the mobile phase was 0.3 ml/min with a gradient ranging from 2 to 98% aqueous acetonitrile containing 0.1% formic acid in a 10-min run. TOFMS was operated in both positive and negative modes with electrospray ionization. The source temperature and desolvation temperature were set at 120 and 350°C, respectively. Nitrogen was applied as the cone gas (10 l/h) and desolvation gas (700 l/h) and argon as the collision gas. TOFMS was calibrated with [Glu1]-fibrinopeptide and monitored by the intermittent injection of lock mass leucine enkephalin in real time. The capillary voltage and the cone voltage were set at 3.5 kV and 35 V in positive ion mode. Screening and identification of major metabolites were performed by using MarkerLynx software (Waters) based on accurate mass measurement (mass errors less than 10 ppm). The structures of TPV and its metabolites were elucidated by tandem mass spectrometry fragmentation with collision energy ramp ranging from 10 to 30 eV.

Data Analysis. Mass chromatograms and mass spectra were acquired by MassLynx software in centroid format from *m/z* 50 to *m/z* 1000. Centroid and integrated mass chromatographic data were processed by MarkerLynx software to generate a multivariate data matrix. Principal component analysis (PCA) and orthogonal projection to latent structures-discriminant analysis (OPLS-DA) were conducted on Pareto-scaled data. The corresponding data matrices were then exported into SIMCA-P+ (version 12; Umetrics, Kinnelon, NJ) for multivariate data analysis.

Results

TPV Metabolic Profiles in Mice. TPV and its metabolites were found in feces but not in urine. The results of chemometric analysis on the ions produced by UPLC-TOFMS assay of control and TPV-treated mouse feces are shown in Fig. 1. The unsupervised PCA analysis score plot (Fig. 1A) revealed two clusters corresponding to the control and TPV-treated groups. The corresponding S-plot (Fig. 1B) generated from OPLS-DA displays the ion contribution to this group separation. The ions associated with TPV treatment that contributed to group separation were TPV and its metabolites, which were marked in the S-plot (Fig. 1B). The chromatograms of TPV and its metabolites are presented in Fig. 1C.

Identification of TPV Metabolites in Feces. *Monohydroxylated TPV metabolites.* Three TPV monohydroxylated metabolites (II, III, and IV) were observed. Metabolite II eluted at 6.32 min and had a protonated molecular ion at *m/z* 619, 16 Da higher than that of TPV (Fig. 2A). MS/MS analysis of metabolite II produced daughter ions at *m/z* 427 (loss of $C_{13}H_{18}$ and H_2O) and 391 (loss of $C_6H_3F_3NO_2S$ and H_2O). The daughter ion at *m/z* 362 is derived from the daughter ion at *m/z* 391 by loss of an ethyl group. In addition, the major daughter ions at *m/z* 319 and 109 suggest that the oxidation occurs on the ring of the aniline moiety. The daughter ions of metabolite II are interpreted in the inlaid structural diagram (Fig. 2B).

Metabolite III was detected at a retention time of 5.88 min in the positive ion mode, having a mass of $[M + H]^+ = 619$ *m/z* ($C_{31}H_{33}F_3N_2O_6S$). MS/MS analysis of metabolite III suggested daughter ions at *m/z* 411 and 201 via the same fragmentation patterns as those for TPV (Fig. 2A). Beyond these ions, new fragments were observed at *m/z* 557 (loss of CO_2 and H_2O) and 495 (loss of C_7H_6O and H_2O). The segment at *m/z* 107 implied that the oxidation occurred in the benzyl group. The other ions at *m/z* 601, 391, 349, and 133 are interpreted in Fig. 2C.

Metabolite IV (at a retention time of 6.57 min) had a mass of $[M + H]^+ = 619$ *m/z* ($C_{31}H_{33}F_3N_2O_6S$). The corresponding MS/MS analysis showed the major daughter ions at *m/z* 409 (loss of $C_6H_3F_3NO_2S$) and 391 (loss of $C_6H_3F_3NO_2S$ and H_2O). The fragments at *m/z* 191 and 149 implied that the phenethyl moiety was oxidized. The other daughter ions are interpreted in the inlaid structural diagram (Fig. 2D).

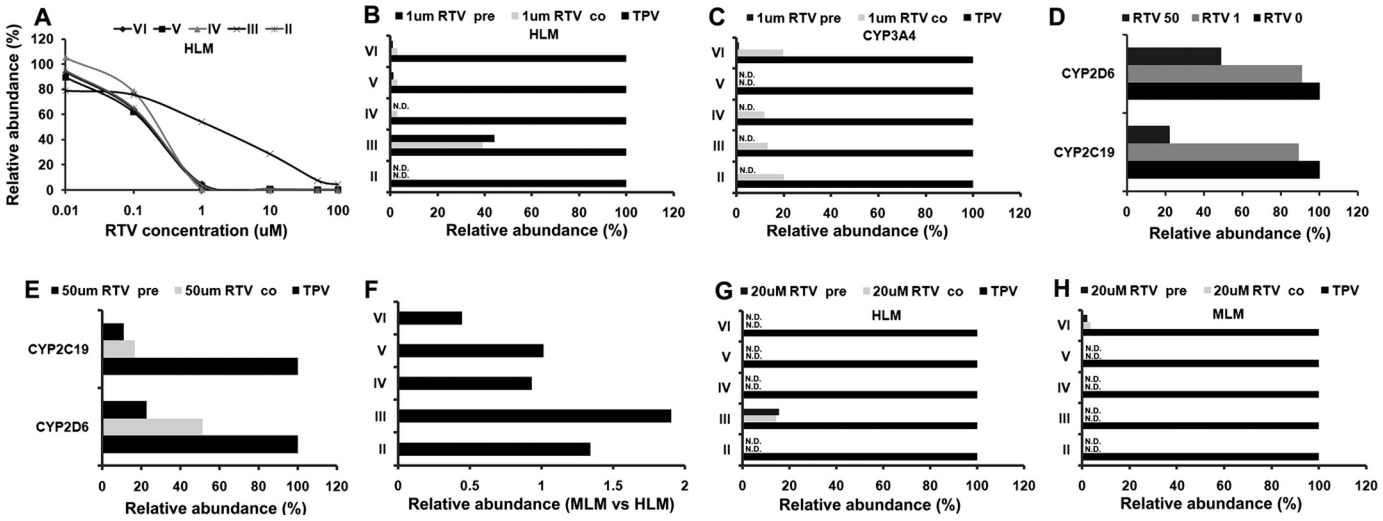

FIG. 3. TPV metabolism in vitro and inhibition by RTV. Duplicate incubations were conducted in 1$\times$ PBS (pH 7.4) containing TPV (50 μM), NADPH (1.0 mM), HLM (0.5 g protein/l) or MLM (0.5 g protein/l), or cDNA-expressed CYP3A4 (10 nM), CYP2D6 (10 nM), and CYP2C19 (10 nM), with coincubation of RTV (RTV co), or preincubation of RTV (RTV pre) respectively. Metabolites II, III, IV, V, and VI were analyzed by UPLC-TOFMS. A, effect of RTV (0–100 μM) on TPV metabolism in HLM. B, effect of preincubation of RTV and coincubation of RTV (1 μM) on TPV metabolism in HLM. C, effect of preincubation of RTV and coincubation of RTV (1 μM) on TPV metabolism in cDNA-expressed CYP3A4. D, effect of coincubation of 1 and 50 μM RTV on TPV metabolism in cDNA-expressed CYP2C19 and CYP2D6. E, effect of preincubation of RTV and coincubation of RTV (50 μM) on TPV metabolism in cDNA-expressed CYP2C19 and CYP2D6 (10 nM). F, comparison of TPV metabolism in HLM and MLM. The overall abundance of TPV metabolites was set as 100% in the incubation of HLM and MLM. The relative abundance of each metabolite was compared and is presented as relative ratio (MLM versus HLM). G, effect of preincubation of RTV and coincubation of RTV (20 μM) on TPV metabolism in HLM. H, effect of preincubation of RTV and coincubation of RTV (20 μM) on TPV metabolism in MLM (10 nM). The data are expressed as means. For each metabolic pathway, the incubation without RTV was set as 100%. N.D., not detected. The metabolite identification was accordant with that in Figs. 2 and 6.

Depropylated TPV metabolite. The structural elucidation of depropyl-TPV (metabolite V) is shown in Fig. 2E, with major daughter ions at *m/z* 543 (loss of H_2O), 479 (loss of C_2F_3), 333 (loss of $C_6H_3F_3NO_2S$ and H_2O), and 291 (loss of $C_6H_3F_3NO_2S$, CO_2, and H_2O). The fragmentation of TPV is depicted in Fig. 2A, with daughter ions at *m/z* 585 (loss of H_2O), 521 (loss of C_2F_3), 375 (loss of $C_6H_3F_3NO_2S$ and H_2O), and 333 (loss of $C_6H_3F_3NO_2S$, CO_2, and H_2O). After the loss of the same moieties, all of the peaks as above in metabolite V had 42 mass units less than those of TPV so it was tentatively identified as depropyl-TPV.

Dehydrogenated TPV metabolites. The three dehydrogenated metabolites (VI, VII, and VIII) were detected in the feces. Metabolite VI (at a retention time of 7.44 min) corresponded to a protonated molecular ion at *m/z* 601, 2 mass units less than that of TPV. Therefore, metabolite VI appeared to be a dehydrogenated metabolite. As shown in Fig. 2F, MS/MS of metabolite VI produced daughter ions at *m/z* 391 (loss of $C_6H_3F_3NO_2S$), 173, and 91 (benzyl), which suggested that the dehydrogenation might take place in the propyl moiety of the molecule.

Metabolite VII was eluted at 6.01 min and had a $[M + H]^+ = 601$ *m/z* ($C_{31}H_{31}F_3N_2O_5S$). The daughter ions at *m/z* 391 (loss of $C_6H_3F_3NO_2S$), 343, 259, and 133 were interpreted in the inlaid structural diagram. The dehydrogenation of metabolite VII may occur in the encircled unit in Fig. 2G.

The third desaturated metabolite (VIII) was observed at a retention time of 6.11 min, having a protonated molecular ion at *m/z* 601. The fragment ions at *m/z* 391 (loss of $C_6H_3F_3NO_2S$) and 213 are interpreted in Fig. 2H. The formation of daughter ions at *m/z* 199 and 133 suggested that dehydrogenation probably took place in the phenylethyl moiety of the molecule.

Dihydroxylated TPV metabolite. A mass of $[M + H]^+ = 635$ *m/z* was noted and corresponded to the empirical formula ($C_{31}H_{33}F_3N_2O_7S$) for dihydroxytipranavir (metabolite IX). The dihydroxylation metabolite had a shorter retention time (5.76 min) than those for all of the TPV monohydroxylation metabolites. MS/MS of metabolite IX produced the daughter ions at *m/z* 573 ($-CO_2$, $-H_2O$), 425 (loss of $C_6H_3F_3NO_2S$), 407 (loss of $C_6H_3F_3NO_2S$ and H_2O), 191, and 149. The formation of daughter ions at *m/z* 425, 191, 107, and 149 suggested that the hydroxylations occurred in the aniline moiety and benzyl unit, respectively (Fig. 2I).

Role of P450s in TPV Metabolism and Inhibition by RTV. Among these eight TPV metabolites, five of them were recapitulated in the in vitro study using HLM (Fig. 3A), including three monohydroxylated metabolites (II, III, and IV), one desaturated metabolite (VI), and one dealkylated metabolite (V). All of these TPV metabolic pathways in HLM were NADPH-dependent. The incubation of TPV with nine different human cDNA-expressed P450s revealed that CYP3A4 was the primary enzyme contributing to the metabolic pathways of metabolites II, IV, V, and VI (Table 1). All other P450s showed little or no activity for metabolites II, IV, V, and VI. Multiple enzymes were involved in the metabolic pathway of metabolite III with the metabolic rate mediated by CYP2D6 > CYP2C19 > CYP3A4 > CYP2C8 (Table 1). The inhibitory effect of RTV on these TPV metabolic pathways was verified by preincubation and coincubation of RTV with HLM, MLM, cDNA-expressed CYP3A4, CYP2D6, and CYP2C19. RTV strongly inhibited metabolic pathways of metabolites II, IV, V, and VI as a half-maximal inhibitory concentration (IC_{50}) less than 0.5 μM in HLM (Fig. 3A). At 1 μM RTV, greater than 80% formation of metabolites II, IV, V, and VI in HLM was suppressed (Fig. 3B). All five CYP3A4-mediated TPV metabolic pathways were significantly suppressed by coincubation of RTV at 1 μM (Fig. 3C). The preincubation of RTV (1.0 μM) with HLM or CYP3A4 more effectively inhibited the formation of metabolites than the coincubation for metabolites II, IV, V, and VI (Fig. 3C). At 1 μM, the CYP3A4-mediated formation of metabolites II, III, IV, V, and VI was almost 100% inhibited by preincubation of RTV (Fig. 3C).

TABLE 1

Roles of P450s in TPV metabolic pathways

Duplicate incubations were conducted in 1× PBS (pH 7.4) containing TPV (50 μM), NADPH (1.0 mM), and each cDNA-expressed P450 enzyme (10 nM). Metabolites were analyzed by UPLC-TOFMS. The highest peak area of each metabolite produced by a cDNA-expressed P450 was set as 100%, and the contribution of others was compared with this enzyme. The data are expressed as means. The metabolite identification was accordant with Figs. 2 and 6.

	II	III	IV	V	VI
			%		
Control	0	0	0	0	0
CYP1A2	0	0	0	0	0
CYP2A6	5.6	0	0	0	0
CYP2B6	0	0	0	0	0
CYP2C8	0	13	0	0	1.1
CYP2C9	0	0	0	0	0
CYP2C19	0	60	0	0	0
CYP2D6	0	100	0	0	0
CYP2E1	0	0	0	0	0
CYP3A4	100	27	100	100	100

The inhibitory effect of RTV on metabolite III formation was different from that of metabolites II, IV, V, and VI. RTV at 1 μM only inhibited ~60% of metabolite III formation in HLM (Fig. 3B). The IC_{50} of RTV for metabolite III formation was ~10-fold higher than that of metabolites II, IV, V, and VI in HLM (Fig. 3A). Preincubation and coincubation of RTV had a similar inhibitory effect on the formation of metabolite III in HLM (Fig. 3B). At 1 μM RTV had no significant effect on the formation of metabolite III when it was coincubated with CYP2D6 and CYP2C19 (Fig. 3D). When the RTV concentration was increased to 50 μM, the formation of metabolite III was suppressed by ~50% during incubation with CYP2D6 and ~80% during incubation with CYP2C19 (Fig. 3D). The more significant inhibition of metabolite III formation was noted when RTV was preincubated with CYP2C19 and CYP2D6 (Fig. 2E).

Five metabolites of TPV were also observed in MLM. A similar level of TPV metabolism in HLM and in MLM was noted (Fig. 3F). To mimic the human dose ratio of TPV and RTV (5:2), inhibitory experiments were performed in HLM and MLM with 50 μM TPV and 20 μM RTV. The formation of TPV metabolites II, IV, V, and VI in HLM was completely suppressed by preincubation or coincubation with 20 μM RTV, and more than 80% formation of metabolite III was inhibited (Fig. 3G). In MLM, the formation of metabolites II, III, IV, and V in MLM was totally inhibited by preincubation or coincubation with 20 μM RTV, and ~90% of formation of metabolite VI was inhibited (Fig. 3H).

Effect of RTV on TPV Metabolism and Tissue Distribution. The tissue distribution of TPV is illustrated in Fig. 4A. The highest distribution is in the liver, followed by the kidney, spleen, and lung. A small amount of TPV was detected in the brain and eyes. RTV had tissue distribution similar to that of TPV, with the liver having the highest concentration (Fig. 4B). In TPV/r-cotreated mice, the TPV abundance in the liver, spleen, and eyes was significantly higher than that in mice treated with TPV alone (Fig. 4A). All eight TPV metabolites identified from the feces were detected in the serum and liver of the mice. If we assume a basis of 100% for TPV and its metabolites in each tissue, TPV metabolites accounted for 31 and 38% in the serum and liver in the TPV-alone group (Fig. 5A and B). In TPV/r-cotreated mice, only 1 and 2% of metabolites were detected in the serum and liver (Fig. 5, C and D).

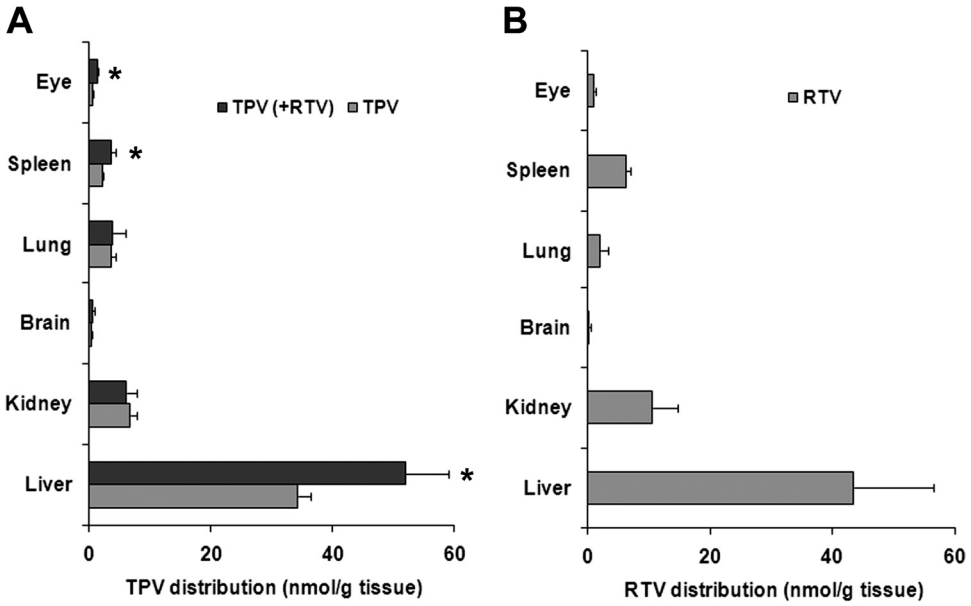

FIG. 4. TPV and RTV tissue distribution in mice. Mice were treated orally with TPV (100 mg/kg), RTV (40 mg/kg), or TPV/r (100/40 mg/kg), respectively. Tissues including liver, brain, lung, kidney, spleen, and eyes were collected 30 min after treatment. TPV and RTV were extracted and analyzed by UPLC-TOFMS. A, TPV tissue distribution in TPV-treated and TPV/r-cotreated mice. B, RTV tissue distribution in TPV/r-cotreated mice. The data are expressed as means ± S.D. ($n = 4$). *, $P < 0.05$ versus TPV-treated mice.

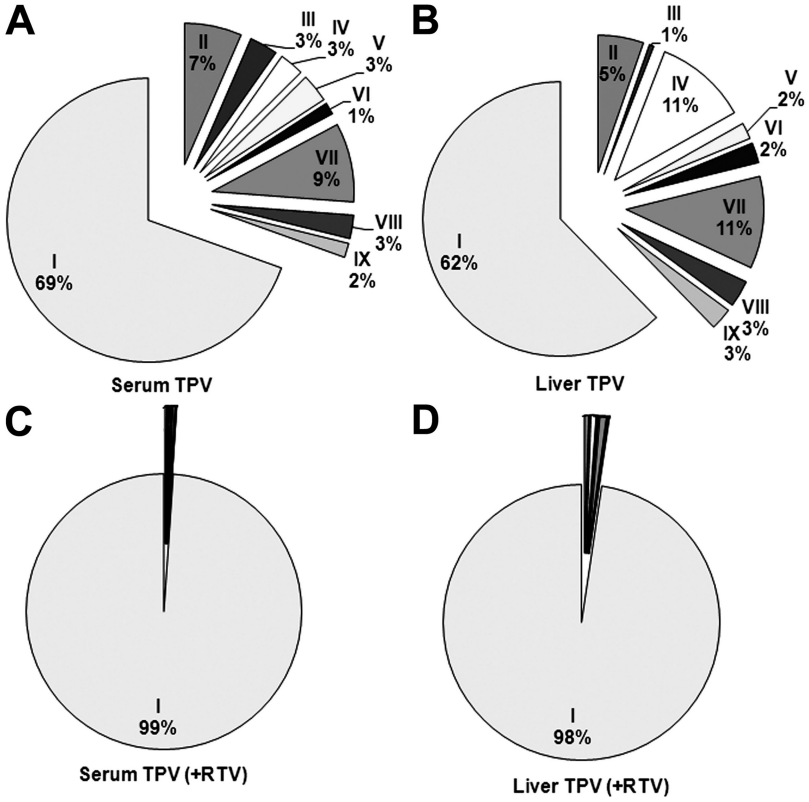

FIG. 5. Relative quantification of TPV and its metabolites in liver and serum from TPV-treated and TPV/r-cotreated mice. TPV and its metabolites were analyzed by UPLC-TOFMS. The overall abundance of TPV and its metabolites was set as 100% in each tissue. The data are expressed as means ($n = 4$). The metabolite identification is accordant with that in Figs. 2 and 6. A, TPV and its metabolites in the serum of TPV-treated mice. B, TPV and its metabolites in the liver of TPV-treated mice. C, TPV and its metabolites in the serum of TPV/r-cotreated mice. D, TPV and its metabolites in the liver of TPV/r-cotreated mice.

Discussion

Traditionally, radiotracing is an efficient method for performing drug metabolism tests. However, its application is limited because of the source of radiolabeled compounds as well as concerns about environmental contamination and safety. In recent years, applicability of the metabolomic approach, which does not need radiolabeled compounds, in drug metabolism has been well established (Chen et al., 2007a). In the current study, TPV metabolism in mice was investigated using a metabolomic approach. Analysis of urine and feces revealed that TPV and its metabolites were mainly excreted in the feces. This finding is in accordance with previous studies using radiolabeled TPV. In previous studies, two monohydroxylated metabolites, one dehydrogenated metabolite, and one glucuronide-conjugated metabolite have been reported (Chen et al., 2007b; Macha et al., 2007). In these reports, one hydroxylation took place in a benzyl group, and the other hydroxylation occurred in a trifluoromethyl-substituted pyridinyl ring. Our data indicated that one monohydroxylation took place on an aniline ring (II) and the other two occurred in a benzyl group (metabolites III and IV). In addition, three dehydrogenated metabolites were observed, with one of them (metabolite VII) corresponding to the previously reported metabolite and the other two (metabolites VI and VIII) being novel metabolites. Metabolite VIII may derive from the hydroxylated metabolites III or IV by loss of water. Furthermore,

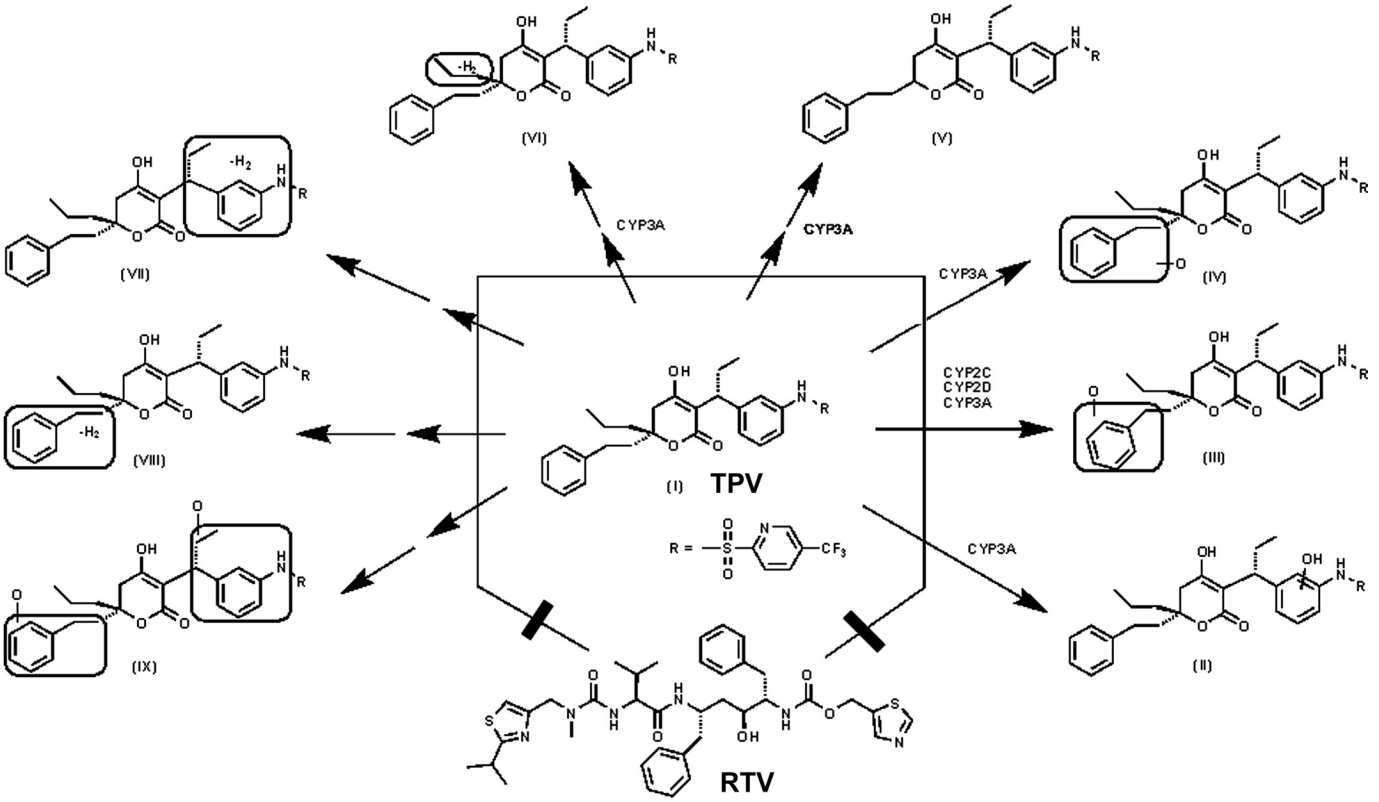

FIG. 6. TPV metabolism and inhibition by RTV in mice. By using a metabolomic approach, the TPV metabolic map was extended to include two known and six novel pathways. CYP3A was identified as the primary enzyme contributing to the formation of four TPV metabolites (II, IV, V, and VI). CYP2C, CYP2D, and CYP3A have collaboratively contributed to the formation of a monohydroxylated metabolite (III). All TPV metabolic pathways were significantly inhibited by RTV in vivo.

dihydroxylated TPV (metabolite IX) was uncovered. It is interesting to note that a CYP3A-mediated carbon-carbon bond cleavage (metabolite V) was found in TPV metabolism in both the mouse and HLM. This type of carbon-carbon cleavage was reported by Brandon et al. (2005, 2006), but the mechanism underlying this type of carbon-carbon cleavage is not clear.

Among the eight metabolites observed in the feces of mice, five metabolites, consisting of three monohydroxylated metabolites (II, III, and IV), one desaturated metabolite (VI), and one depropylated metabolite (V), were recapitulated in HLM. Incubation of TPV with recombinant P450s demonstrated that CYP3A4 was the primary enzyme contributing to the metabolic pathways of metabolites II, IV, V, and VI. Multiple P450s involved in the metabolic pathway of metabolite III included CYP2D6, 2C19, 3A4, and 2C8. TPV metabolites VII, VIII, and IX were only detected in the in vivo study, and the roles of P450s on these pathways were not confirmed. However, the data from TPV/r cotreatment suggest that the enzymes contributing to the formations of metabolites VII, VIII, and IX could have been inhibited by RTV. RTV inhibition of the TPV metabolic pathway of metabolite III was different from that of metabolites II, IV, V, and VI because different enzymes contributed to the metabolic pathways. RTV selectively inhibits CYP3A activity at low concentrations. With increasing concentrations, RTV inhibits CYP2C, CYP2D, and CYP3A activities (Eagling et al., 1997; von Moltke et al., 1998; Vourvahis and Kashuba, 2007). The mechanism of inhibition of RTV was identified by the preexposure of RTV in HLM, MLM, and cDNA-expressed enzymes (CYP3A4, CYP2C19, and CYP2D6, respectively). Our data suggested that RTV-mediated inhibition of TPV metabolism occurs in a mechanism-based manner, which is consistent with the previous report (Koudriakova et al., 1998; Ernest et al., 2005). In addition, we demonstrated that TPV metabolism in HLM and MLM is similar; therefore, the experiment in mice can be extrapolated to humans.

TPV is an efficient drug for the treatment of drug-experienced patients resistant to other PIs (Temesgen and Feinberg, 2007). However, TPV/r cotherapy can lead to intracranial hemorrhage and hepatotoxicity. More than 10 cases of intracranial hemorrhage and 12 cases of liver-associated deaths were reported from the Food and Drug Administration. Assessment of risk/benefit of a TPV/r regimen is suggested for patients at risk for intracranial hemorrhage and hepatic failure (Chan-Tack et al., 2008). The mechanism of TPV/r toxicity is not completely clear. We noted that TPV was highly concentrated in the liver, especially when cotreated with RTV. In addition, biliary excretion seems to be critical for TPV and its metabolites, because they were only detected in feces. These data indicate that disruption of biliary function may predispose a patient to a risk for TPV-induced liver injury. Compared with the liver, the brain has extremely low TPV distribution, which suggests that TPV-related intracranial hemorrhage may be due to indirect toxicity of TPV/r. Further studies are needed to establish a mechanism of TPV/r induced intracranial hemorrhage and hepatotoxicity.

In summary, TPV metabolism was thoroughly investigated in mice by using a metabolomic approach, and the TPV metabolic map was extended to include two known and six novel pathways (Fig. 6). CYP3A was identified as the primary enzyme contributing to the formation of four TPV metabolites, including one with an unusual carbon-carbon bond cleavage. CYP2C, CYP2D, and CYP3A have collaboratively contributed to the formation of a monohydroxylated metabolite (metabolite III). RTV inhibited CYP2C-, CYP2D-, and CYP3A-mediated TPV metabolism. In vivo, RTV cotreatment significantly inhibited all eight TPV metabolic pathways, which indicated

that the RTV-mediated boosting of TPV is due to the modulation of P450-dependent metabolism.

Acknowledgments. We thank the National Institutes of Health AIDS Research and Reference Reagent Program for providing TPV and RTV; Dr. Curtis D. Klaassen for expert advice; and Nazia Ali for editing the manuscript.

References

Brandon EF, Sparidans RW, Guijt KJ, Löwenthal S, Meijerman I, Beijnen JH, and Schellens JH (2006) In vitro characterization of the human biotransformation and CYP reaction phenotype of ET-743 (Yondelis, Trabectidin), a novel marine anti-cancer drug. *Invest New Drugs* **24:**3–14.

Brandon EF, van Ooijen RD, Sparidans RW, Lázaro LL, Heck AJ, Beijnen JH, and Schellens JH (2005) Structure elucidation of aplidine metabolites formed in vitro by human liver microsomes using triple quadrupole mass spectrometry. *J Mass Spectrom* **40:**821–831.

Cahn P, Villacian J, Lazzarin A, Katlama C, Grinsztejn B, Arasteh K, López P, Clumeck N, Gerstoft J, Stavrianeas N, et al. (2006) Ritonavir-boosted tipranavir demonstrates superior efficacy to ritonavir-boosted protease inhibitors in treatment-experienced HIV-infected patients: 24-week results of the RESIST-2 trial. *Clin Infect Dis* **43:**1347–1356.

Chan-Tack KM, Struble KA, and Birnkrant DB (2008) Intracranial hemorrhage and liver-associated deaths associated with tipranavir/ritonavir: review of cases from the FDA's Adverse Event Reporting System. *AIDS Patient Care STDS* **22:**843–850.

Chen C, Gonzalez FJ, and Idle JR (2007a) LC-MS-based metabolomics in drug metabolism. *Drug Metab Rev* **39:**581–597.

Chen C, Meng L, Ma X, Krausz KW, Pommier Y, Idle JR, and Gonzalez FJ (2006) Urinary metabolite profiling reveals CYP1A2-mediated metabolism of NSC686288 (aminoflavone). *J Pharmacol Exp Ther* **318:**1330–1342.

Chen L, Sabo JP, Philip E, Mao Y, Norris SH, MacGregor TR, Wruck JM, Garfinkel S, Castles M, Brinkman A, et al. (2007b) Steady-state disposition of the nonpeptidic protease inhibitor tipranavir when coadministered with ritonavir. *Antimicrob Agents Chemother* **51:**2436–2444.

Courter JD, Girotto JE, and Salazar JC (2008) Tipranavir: a new protease inhibitor for the pediatric population. *Expert Rev Anti Infect Ther* **6:**797–803.

Eagling VA, Back DJ, and Barry MG (1997) Differential inhibition of cytochrome P450 isoforms by the protease inhibitors, ritonavir, saquinavir and indinavir. *Br J Clin Pharmacol* **44:**190–194.

Ernest CS, 2nd, Hall SD, and Jones DR (2005) Mechanism-based inactivation of CYP3A by HIV protease inhibitors. *J Pharmacol Exp Ther* **312:**583–591.

Giri S, Idle JR, Chen C, Zabriskie TM, Krausz KW, and Gonzalez FJ (2006) A metabolomic approach to the metabolism of the areca nut alkaloids: arecoline and arecaidine in the mouse. *Chem Res Toxicol* **19:**818–827.

Hsu A, Granneman GR, and Bertz RJ (1998) Ritonavir. Clinical pharmacokinetics and interactions with other anti-HIV agents. *Clin Pharmacokinet* **35:**275–291.

Kempf DJ, Marsh KC, Kumar G, Rodrigues AD, Denissen JF, McDonald E, Kukulka MJ, Hsu A, Granneman GR, Baroldi PA, et al. (1997) Pharmacokinetic enhancement of inhibitors of the human immunodeficiency virus protease by coadministration with ritonavir. *Antimicrob Agents Chemother* **41:**654–660.

Koudriakova T, Iatsimirskaia E, Utkin I, Gangl E, Vouros P, Storozhuk E, Orza D, Marinina J, and Gerber N (1998) Metabolism of the human immunodeficiency virus protease inhibitors indinavir and ritonavir by human intestinal microsomes and expressed cytochrome P4503A4/3A5: mechanism-based inactivation of cytochrome P4503A by ritonavir. *Drug Metab Dispos* **26:**552–561.

Ma X, Chen C, Krausz KW, Idle JR, and Gonzalez FJ (2008) A metabolomic perspective of melatonin metabolism in the mouse. *Endocrinology* **149:**1869–1879.

MacGregor TR, Sabo JP, Norris SH, Johnson P, Galitz L, and McCallister S (2004) Pharmacokinetic characterization of different dose combinations of coadministered tipranavir and ritonavir in healthy volunteers. *HIV Clin Trials* **5:**371–382.

Macha S, Chen L, Norris SH, Philip E, Mao Y, Silverstein H, Struble C, and Beers W (2007) Biotransformation and mass balance of tipranavir, a nonpeptidic protease inhibitor, when co-administered with ritonavir in Sprague-Dawley rats. *J Pharm Pharmacol* **59:**1223–1233.

McCallister S, Valdez H, Curry K, MacGregor T, Borin M, Freimuth W, Wang Y, and Mayers DL (2004) A 14-day dose-response study of the efficacy, safety, and pharmacokinetics of the nonpeptidic protease inhibitor tipranavir in treatment-naive HIV-1-infected patients. *J Acquir Immune Defic Syndr* **35:**376–382.

Pham PA (2005) FDA approves Aptivus (tipranavir). *Hopkins HIV Rep* **17:**6–7.

Temesgen Z and Feinberg J (2007) Tipranavir: a new option for the treatment of drug-resistant HIV infection. *Clin Infect Dis* **45:**761–769.

Thomas GH (2001) Metabolomics breaks the silence. *Trends Microbiol* **9:**158.

von Moltke LL, Greenblatt DJ, Grassi JM, Granda BW, Duan SX, Fogelman SM, Daily JP, Harmatz JS, and Shader RI (1998) Protease inhibitors as inhibitors of human cytochromes P450: high risk associated with ritonavir. *J Clin Pharmacol* **38:**106–111.

Vourvahis M and Kashuba AD (2007) Mechanisms of pharmacokinetic and pharmacodynamic drug interactions associated with ritonavir-enhanced tipranavir. *Pharmacotherapy* **27:**888–909.

Weckwerth W (2003) Metabolomics in systems biology. *Annu Rev Plant Biol* **54:**669–689.

Address correspondence to: Dr. Xiaochao Ma, Department of Pharmacology, Toxicology and Therapeutics, University of Kansas Medical Center, Kansas City, KS 66160. E-mail: xma2@kumc.edu